Magnetic structure of Yb_2Pt_2Pb: Ising moments on the Shastry-Sutherland lattice

W. Miiller,[1] L. S. Wu,[1] M. S. Kim,[1] T. Orvis,[1] J. W. Simonson,[1] M. Gamża,[2] D. M. McNally,[1] C. S. Nelson,[3] G. Ehlers,[4] A. Podlesnyak,[4] J. S. Helton,[5] Y. Zhao,[5,6] Y. Qiu,[5,6] J. R. D. Copley,[5] J. W. Lynn,[5] I. Zaliznyak,[2] and M. C. Aronson[1,2,*]

[1]*Department of Physics and Astronomy, Stony Brook University, Stony Brook, New York 11794, USA*

[2]*Condensed Matter Physics and Materials Science Department, Brookhaven National Laboratory, Upton, New York 11973, USA*

[3]*National Synchrotron Light Source, Brookhaven National Laboratory, Upton, New York 11973, USA*

[4]*Quantum Condensed Matter Division, Oak Ridge National Laboratory, Oak Ridge, Tennessee 37831, USA*

[5]*NIST Center for Neutron Research, Gaithersburg, Maryland 20899, USA*

[6]*Department of Materials Science and Engineering, University of Maryland, College Park, Maryland 20742, USA*

(Received 8 July 2014; revised manuscript received 12 December 2015; published 22 March 2016)

Neutron diffraction measurements were carried out on single crystals and powders of Yb_2Pt_2Pb, where Yb moments form two interpenetrating planar sublattices of orthogonal dimers, a geometry known as Shastry-Sutherland lattice, and are stacked along the c axis in a ladder geometry. Yb_2Pt_2Pb orders antiferromagnetically at $T_N = 2.07$ K, and the magnetic structure determined from these measurements features the interleaving of two orthogonal sublattices into a $5 \times 5 \times 1$ magnetic supercell that is based on stripes with moments perpendicular to the dimer bonds, which are along (110) and (−110). Magnetic fields applied along (110) or (−110) suppress the antiferromagnetic peaks from an individual sublattice, but leave the orthogonal sublattice unaffected, evidence for the Ising character of the Yb moments in Yb_2Pt_2Pb that is supported by point charge calculations. Specific heat, magnetic susceptibility, and electrical resistivity measurements concur with neutron elastic scattering results that the longitudinal critical fluctuations are gapped with $\Delta E \simeq 0.07$ meV.

DOI: 10.1103/PhysRevB.93.104419

Much attention is focused on coupled spin-dimer systems, where frustrated magnetic interactions can lead to spin liquid ground states [1,2]. The Shastry-Sutherland lattice (SSL), consisting of planes of orthogonal dimers with intradimer exchange J and interdimer exchange J', is of particular interest as it has been exactly solved [3] to show that the ground state is ordered antiferromagnetically (AF) for J/J' less than a critical value $(J/J')_C$ and otherwise has a singlet ground state with gapped magnetic excitations. Insulating $SrCu_2(BO_3)_2$ is an example of the SSL dimer liquid ground state [4–6]. Here, frustrated exchange interactions tend to localize singlet and triplet dimers into complex ordered superstructures at high fields [7–9], resulting in quantized plateaus in the magnetic field B dependence of the magnetization $M(B)$ [10–12].

Most SSL systems are magnetically ordered, where the closure of the singlet dimer gap yields a nonzero magnetization that makes AF order possible even for $B = 0$. The metallic RB_4 (R = Ho,Er,Tm,Tb) compounds order AF with period-doubling Néel ground states with Ising-like moments oriented perpendicular to the SSL planes [13–16]. In metallic Yb_2Pt_2Pb, Yb moments form the orthogonal dimers of the SSL planes, and AF order appears below the Néel temperature $T_N = 2.07$ K [17]. The exchange interactions $J \simeq 5$ K and $J/J' \simeq 1$ deduced from the magnetic susceptibility $\chi(T)$ [18] are much smaller in Yb_2Pt_2Pb than in the RB_4, and a field of only 1.23 T, applied along the (110) or (−110) dimer bond directions, partially suppresses the $B = 0$ AF order, accompanied by quantized $M(B)$ steps [18–20] that culminate in the saturation of $M(B)$ at $\simeq 3$ T. The magnetic structures of SSL systems reflect the frustration of short-ranged magnetic interactions, and in Yb_2Pt_2Pb, where the Yb moments are large and classical with strong Ising anisotropy that confines them to the SSL plane, we can expect AF states that are analogous to but distinct from those found in $SrCu_2(BO_3)_2$ at high fields, where Heisenberg quantum spins $S = 1/2$ are aligned perpendicular to the SSL layers.

The neutron diffraction measurements presented here demonstrate that the in-plane Ising-like Yb moments in Yb_2Pt_2Pb have a remarkably complex magnetic structure, with a commensurate superlattice of ordered stripes consisting of moment-bearing and magnetically compensated Yb pairs with moments perpendicular to the (110) and (−110) dimer bonds. The magnetic cell contains 200 Yb atoms, whose Ising character results in the formation of two independent and orthogonal sublattices that are separately polarized by magnetic fields along either (110) or (−110). The persistence of AF order in the surviving AF sublattice shows that the two orthogonal bonds of the $B = 0$ SSL are effectively decoupled in magnetic field, leading to a unique high field ground state. The development of the AF order parameter in Yb_2Pt_2Pb is mirrored in the temperature dependencies of the specific heat C/T and the temperature derivatives of the magnetic susceptibility $\chi(T)$ and electrical resistivity $\rho(T)$, suggesting that the stripe-ordered ground state is preceded by the dynamical freezing of longitudinal critical fluctuations that are gapped.

Single crystals of Yb_2Pt_2Pb were grown from Pb flux [17]. Neutron scattering experiments were carried out with an incident neutron wavelength of 2.359 Å on the BT-7 triple axis spectrometer at the NIST Center for Neutron Research (NCNR) [21] on 5 g of powder that was prepared by triturating single crystals, and on a 60 mg single crystal. A single crystal diffraction experiment was performed on this same crystal at 1.8 K on beamline X21 at the National Synchrotron Light Source (NSLS) at Brookhaven National Laboratory, with an incident x-ray energy of 10 keV. Further neutron diffraction data were extracted from the full time of flight data sets

*maronson@bnl.gov

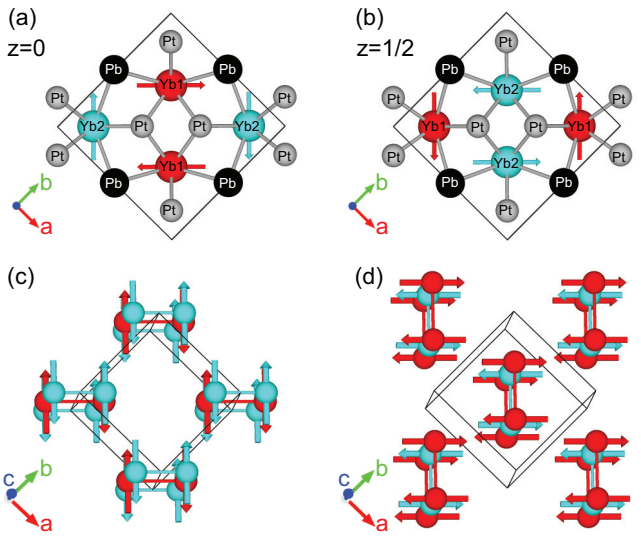

FIG. 1. (a), (b) Chemical environment for Yb1 (red) and Yb2 (blue) sites at the $z = 0$ (a), and the $z = 1/2$ (b) plane, respectively. The nearest Pt (gray) and Pb (black) neighbors are located below and above the $z = 0$ and $z = 1/2$ planes [17]. The red and blue vectors indicate the magnetic moment directions from the point charge model calculation [23,25,26]. (c), (d) Simplified magnetic sublattices with Yb moments along the (-110) direction [sublattice 1, (c)], and along the (110) direction [sublattice 2, (d)].

obtained at the Cold Neutron Chopper Spectrometer (CNCS) at the Spallation Neutron Source and the Disk Chopper Spectrometer (DCS) at NCNR using a 6 g collection of $\sim$300 oriented single crystals of Yb_2Pt_2Pb with an estimated angular mosaic perpendicular to the c axis of $\simeq 2$ degrees. An incident energy $E_i = 3.27$ meV was used at DCS [22], for $T \geqslant 0.1$ K and fields as large as 8 T, while $E_i = 3.32$ meV was used at CNCS for the diffraction study and a higher incident energy of 37 meV was used to to identify crystal field excitations.

The Yb ions in Yb_2Pt_2Pb have an extremely strong Ising anisotropy that has important ramifications for the magnetic structure that we will propose. The crystal structure in the SSL planes [Figs. 1(a) and 1(b)] features Yb1 and Yb2 sites, both having the same $C2v$ ($m2m$) point group symmetry, although the Yb1-Yb1 spacing is 3.545 Å, and the Yb2-Yb2 spacing is 3.889 Å. Each is surrounded by six nearest neighbor Pt atoms (three above and three below the Yb-Yb plane), and four nearest neighbor Pb atoms (two above and two below the Yb-Yb plane) [17]. These Pt and Pb atoms provide an anisotropic environment of static charges that lifts the eightfold degeneracy of the $J = 7/2$ multiplet of Yb^{3+}, producing four doublet states for both the Yb1 and Yb2 ions. We have identified the wave functions of the states split by the crystalline electric field (CEF) associated with this point charge model using the software MCPHASE [23–26], in terms of the angular momentum j_z states $|\pm 7/2\rangle$, $|\pm 5/2\rangle$, $|\pm 3/2\rangle$, and $|\pm 1/2\rangle$. As is evident in Figs. 1(a) and 1(b), the high symmetry directions for the Yb1 and Yb2 sites do not coincide with the crystalline axes a, b, and c. For Yb1 sites in the $z = 0$ plane, the eigenstates are most nearly diagonalized by choosing the new axis to be along the $(1, -1, 0)$ direction, and the resulting CEF levels are

$$|E_\pm\rangle_0 = 0.992|\pm 7/2\rangle + 0.100|\pm 3/2\rangle + 0.064|\mp 1/2\rangle + 0.032|\mp 5/2\rangle, \quad (1)$$

$$|E_\pm\rangle_1 = -0.082|\pm 7/2\rangle + 0.300|\pm 3/2\rangle + 0.355|\mp 1/2\rangle + 0.881|\mp 5/2\rangle, \quad (2)$$

$$|E_\pm\rangle_2 = 0.092|\pm 7/2\rangle + 0.785|\pm 3/2\rangle + 0.420|\mp 1/2\rangle - 0.446|\mp 5/2\rangle, \quad (3)$$

$$|E_\pm\rangle_3 = -0.153|\pm 7/2\rangle + 0.832|\pm 3/2\rangle - 0.533|\mp 1/2\rangle + 0.005|\mp 5/2\rangle. \quad (4)$$

It is remarkable that the ground state wave function is a nearly pure state of the angular momentum $j_z = |\pm 7/2\rangle$, and it is well separated from the excited doublets $|E_\pm\rangle_1$, $|E_\pm\rangle_2$, and $|E_\pm\rangle_3$ by the energies $\Delta_1 = 37$ meV, $\Delta_2 = 64$ meV, and $\Delta_3 = 94$ meV. Consequently, the low temperature magnetic properties are expected to be dominated by the ground doublet $|E_\pm\rangle_0$, and the magnetic moments and their anisotropy that we calculate for the ground doublet coincide with the values measured in a 14 T field, which is large enough to saturate the magnetization when it lies in the the SSL plane, indeed indicate a pronounced Ising anisotropy:

$$M_{\bar{1}10} \backsimeq \pm 3.95\mu_B/\text{Yb, measured (14 T)} : 3.8\mu_B/\text{Yb}, \quad (5)$$

$$M_{100} \backsimeq \pm 2.8\mu_B/\text{Yb, measured (14 T)} : 2.7\mu_B/\text{Yb}, \quad (6)$$

$$M_{001} \backsimeq \pm 0.2\mu_B/\text{Yb, measured (14 T)} : 0.25\mu_B/\text{Yb}. \quad (7)$$

Inelastic neutron scattering experiments carried out on CNCS find a nondispersing excitation with an energy $Ec = 25.3 \pm 0.1$ meV (Fig. 2), that we identify as a crystal field excitation between the ground and first excited states of the CEF-split manifold of states. Ec is in reasonable agreement with the splitting $\Delta_1 = 37$ meV between the ground doublet and the first excited doublet that was calculated from the point charge model. Despite the metallic character of Yb_2Pt_2Pb, the point charge model localizes charge on the Pt and Pb ions, which could potentially lead to an overestimate of the CEF splitting. At the same time, the determination of $\Delta_1 \simeq 7$ meV from the analysis of a Schottky peak in the specific heat [17,28] may also be compromised to some extent by uncertainties in the phonon background. Despite these qualifications, the experimental data confirm the prediction of the point charge model that the first excited CEF levels in Yb_2Pt_2Pb are energetically well separated from the Ising ground doublets, where the direct measurement from the inelastic neutron scattering spectrum finds that this energy separation is $\Delta_1 \simeq 25$ meV.

The ground state of the crystal field manifold is a Kramers doublet that is a nearly pure state of angular momentum $j_z = |\pm 7/2\rangle$, implying that at low temperatures, the individual Yb moments can only be in one of two antiparallel states that have equal moment magnitudes. The Ising nature of the ground state is protected by its minimal overlap with the wave functions of the energetically remote excited states. The energy of the first excited state $|E_\pm\rangle_1 \simeq 25$ meV sets the scale for rotating the Yb moments away from the (110) and (-110) directions in

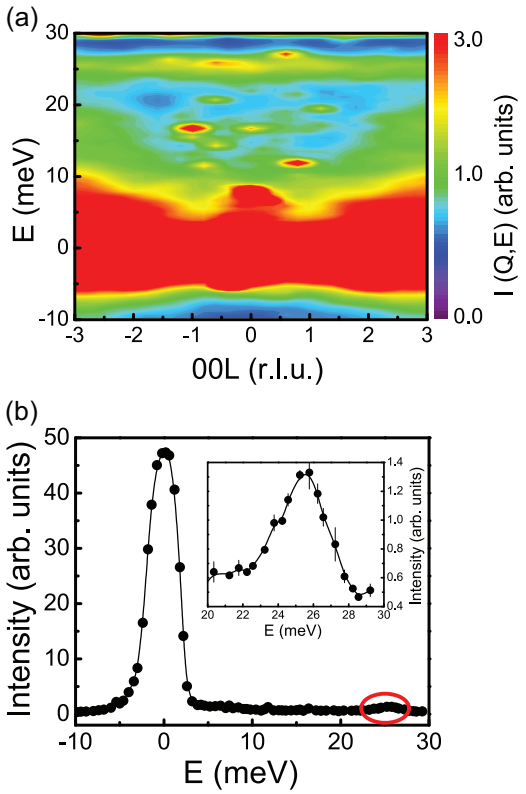

FIG. 2. (a) Contour plot of the inelastic scattering intensity with energy dispersion along the wave vector Q_{00L}, averaged over wave vector $(HH) = [-6,6]$, $(H-H) = [-1,1]$, measured at temperature of $\simeq 175$ K and with an incident energy $E_i = 37$ meV. The scattering at high wave vectors and energies less than 20 meV is due to the aluminum sample holder and cryogenic environment [27]. (b) Energy dependent intensity averaged over wave vector $(HH) = [-3,3]$, $L = [-3,3]$, $(H-H) = [-1,1]$. The inset shows an enlarged plot of the CEF excitation around 25 meV [red circle in (b)].

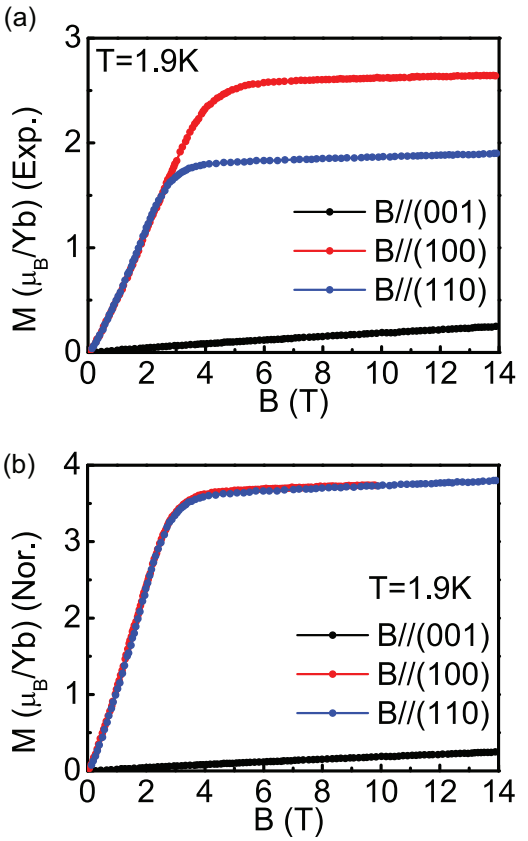

FIG. 3. (a) Experimentally measured magnetization normalized to the formula unit Yb_2Pt_2Pb with field along three principal crystal directions (100), (110), and (001). (b) Magnetization normalized with the two sublattice model as explained in the text. The saturation moment for the field along the diagonal (110) direction is $M_{110}(\text{Nor.}) = 3.8\mu_B/\text{Yb}$, which is much bigger than the moment along the crystal (001) direction with $M_{001}(\text{Nor.}) = 0.25\mu_B/\text{Yb}$ at 14 T at 1.9 K.

the SSL plane, and so at low temperatures no moment canting is permitted and no spiral-type modulated structure of the Yb moments is possible [29–32]. Although the Yb1 and Yb2 sites have slightly different chemical environments, the Yb-Pt and Yb-Pb distances differ only slightly, and the variation in the associated CEF splitting of the ground manifold on the two sites is small compared to $|E_\pm\rangle_1$. Within the $\simeq 3.6$ meV energy resolution of the CNCS inelastic neutron scattering experiment, and the considerable thermal broadening of the CEF levels at the experimental temperature 175 K, we did not resolve any such additional splitting that would distinguish the Yb1 and Yb2 sites. The magnetic moments are consequently expected to be nearly identical on the Yb1 and Yb2 sites.

Magnetization measurements confirm the results of these calculations [17,19,33], showing that the Yb moments are largely confined to the SSL planes, where the moments form a lattice of orthogonal dimers. Since half of the Yb moments can be fully polarized by magnetic fields along (110) or (−110), it has been suggested that there are two orthogonal but otherwise equivalent sublattices in Yb_2Pt_2Pb, each containing half of the Yb moments [19,33]. This too can be explained on the basis of the crystal structure, since Figs. 1(a) and 1(b) show that the chemical environment of the Yb2 sites is rotated 90° with respect to that of the Yb1 sites, and so the magnetic moments of the Yb1 and Yb2 sites are also expected to be orthogonal within the SSL ab planes. Figure 1 demonstrates that Yb1 and Yb2 moments are alternated along the c axis, leading to sublattice 1 with moments along $(1\,-1\,0)$ [Fig. 1(c)], consisting of Yb1 moments in the $z = 0$ plane and Yb2 moments in the $z = 1/2$ planes, while sublattice 2 has moments along (110) [Fig. 1(d)], consisting of Yb2 moments in the $z = 0$ plane and Yb1 moments in the $z = 1/2$ planes. The two sublattices together form the magnetic ab planes, where in a given plane one sublattice is formed entirely of Yb1 moments and the other sublattice is formed entirely from Yb2 moments.

Measurements of the magnetization curves $M(B)$ with the field oriented along (110), (100), and (001) [Fig. 3(a)] are compared to the results of the point charge model in Fig. 3(b). Due to the strong Ising anisotropy of Yb_2Pt_2Pb, a magnetic field larger than $\simeq 2.3$ T oriented along $(1\,-1\,0)$, or (110), readily polarizes one sublattice, while the orthogonal sublattice is nearly unaffected. If we normalize the measured magnetization by the number of moments per formula unit that have their local Ising axes parallel to magnetic field,

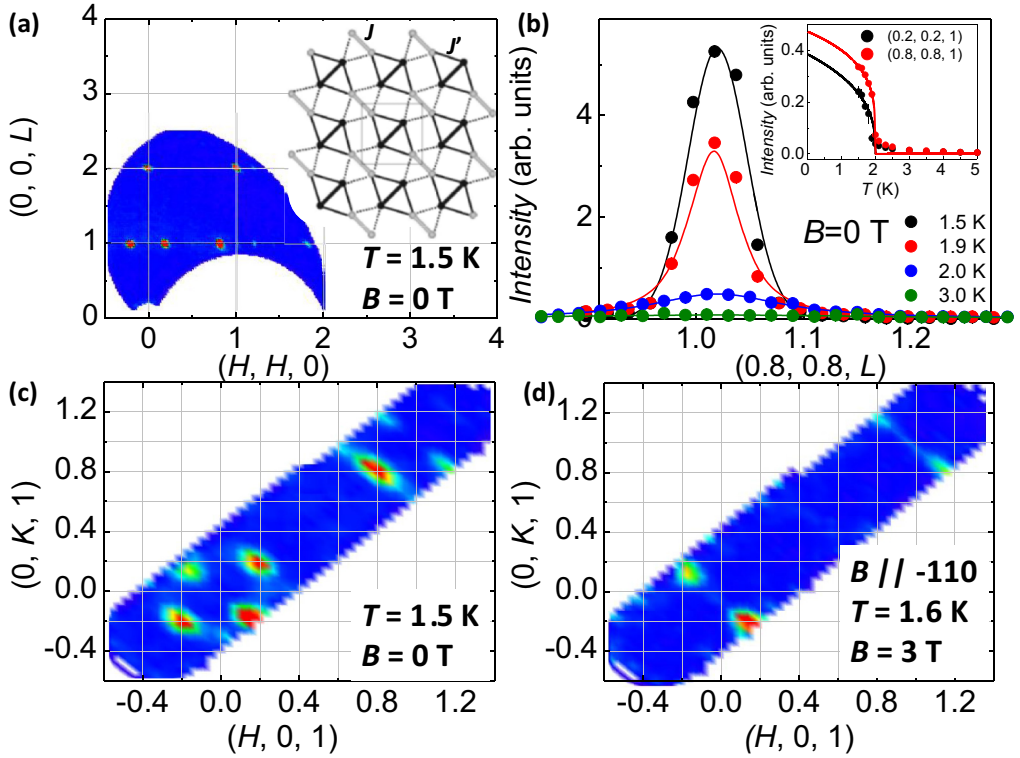

FIG. 4. (a) Contour plot of elastic scattering in HHL plane at 1.5 K. Inset shows orthogonal Yb dimers forming SSL, with dimer bonds along the (110) and (−110) directions. (b) Intensity of the (0.8,0.8,1) AF peak at different temperatures, as indicated. Inset: temperature dependencies of the intensities of the (0.2,0.2,1) (black points) and (0.8,0.8,1) (red points) AF peaks, from which 5 K backgrounds have been subtracted. Solid lines are guides for the eye obtained by fitting intensity to the power law, $I(T) \sim (1 - T/T_N)^{\beta}$, with $\beta \approx 0.12$, which is close to value $\beta = 1/8$ expected for 2D Ising systems. Contour plots of the elastic scattering at 1.5 K in the $(HK1)$ planes for magnetic fields $B = 0$ (c) and $B = 3$ T (d).

we find an experimental value for the saturation moment $M_{110} = 3.8\mu_B$/Yb, which is in close agreement with the value expected from the point charge model, as listed above. The Ising character of the moments is further highlighted by the observation that for a magnetic field applied along (100), the saturation moment M_{100}, is simply the projection of $M_{110} = M_{\bar{1}10} = \sqrt{2} \times M_{100}$. Finally, a magnetic field applied along (001) is perpendicular to all moments, and the small value of M_{001} signals the inability for such a field to induce significant magnetization of the Ising moments, which are constrained to lie in the ab planes. The measured magnetization [Fig. 3(a)] and the results of the point charge model [Fig. 3(b)] are found to be in excellent agreement once the two sublattice character of Yb_2Pt_2Pb is taken into account in this way.

The formation of the antiferromagnetically ordered state in these sublattices destroys the Shastry-Sutherland lattice that was suggested on the basis of the crystal structure in the ab plane [17–20,33]. Figures 3(c) and 3(d) show that each sublattice is a square lattice of dimers with parallel moments that are all Yb1 or all Yb2 type within a given plane, and that these dimers are stacked antiferromagnetically along the c axis into ladders with alternating Yb1-Yb2 rungs. The rungs on neighboring ladders are orthogonal, forming the dimers of the original SSL planes. Much can be predicted about the magnetic moments and their orientation from the crystal structure itself. The essential features that we will use to construct our model of the magnetic structure include two sublattices of orthogonal dimers residing in the ab SSL planes, antiferromagnetic stacking along the c axis, and a strong Ising anisotropy that limits the Yb moments to be along the (110) and (1 − 1 0) directions, with no canting or modulation of the moment magnitude. As we will show, a very satisfactory description of the diffraction data is possible using this model, and in this way we will validate the basic properties of Yb_2Pt_2Pb that were deduced above on the basis of the local chemical environment of the Yb ions.

Neutron diffraction measurements show clear evidence for AF order below $T_N = 2.07$ K [17]. Figure 4(a) is a contour plot of the elastic intensity in the (HHL) scattering plane at 1.5 K, obtained on the collection of aligned Yb_2Pt_2Pb crystals using CNCS. The (002) and (112) nuclear peaks are present at all temperatures, however, satellite peaks emerge around the (001) and (111) Bragg positions for $T \leqslant T_N$. The in-plane AF propagation wave vector $\mathbf{q_1} = (\delta,\delta,0)$ with $\delta = 0.2 \pm 0.02$ in reciprocal lattice units (rlu) is deduced from Gaussian fits to the $(1 - \delta, 1 - \delta, 1)$ superlattice peaks [Fig. 4(b)], indicating that AF order is accompanied by the formation of a $5 \times 5 \times 1$ superstructure. The temperature dependencies of the integrated intensities of the $(\delta,\delta,1)$ and $(1 - \delta, 1 - \delta, 1)$ AF peaks have the appearance of order parameters that are substantially broadened near T_N [Fig. 4(b), inset], although the AF peaks themselves remain sharp.

Our scattering geometry accesses a strip of the $(HK1)$ plane [Fig. 4(c)], where a quartet of AF satellites forms around both

the (001) and (111) Bragg positions. A 3 T magnetic field B applied along (-110) polarizes all antiparallel moments [17,33], and due to the Ising character of the Yb moments, has no effect on perpendicular moments. Figure 4(d) shows that only the AF peaks with $\mathbf{q_1} \parallel B$ survive at 3 T. We first considered the possibility that the quartet of AF satellites [Fig. 4(c)] arises from the presence of two orthogonal twin domains with a single AF wave vector, i.e., spatially extended regions where the AF wave vectors are along 110 in domain type 1 and the orthogonal -110 direction in domain type 2. The minimal constraints that must be accommodated in the two-domain scenario are as follows:

(i) Given their Ising character, the Yb moments can only be perpendicular or parallel to the dimer bonds, which lie along (110) and (-110) directions. (ii) The moment per site can be no larger than $\approx 4.5\mu_B$, which is the maximum Yb moment permitted by Hunds rule. (iii) Both domains should be antiferromagnetic, bearing no net moment in zero field, except perhaps at their boundaries. (iv) All moments in both domains that have a component parallel or antiparallel to the external field will reorient along external fields larger than ≈ 3 T, producing a saturation moment that is consistent with the saturation moment taken from magnetization measurements, which is the equivalent of $\approx 1.9\mu_B$/Yb.

There are three different types of domains 1 and 2, where we consider different configurations of magnetic moments, subject to the above constraints.

In the first case, there is an antiferromagnetic arrangement of moments, which are all perpendicular to the bonds. Given that the bonds are orthogonal, an external field along (110) or (-110) will reorient half of the moments giving the correct saturation moment. However, it is impossible in this case to construct a second type of domain that is not the same as the original domain, via simple translation.

The second scenario takes domain 1 to have moments on the dimer bonds parallel to (110), and these moments can be either parallel or perpendicular to the bonds. Domain 2 also has moments parallel or perpendicular to the (-110) dimer bonds. Here, only half of the bonds in either domain have moments, and in an external field only half of these moments can be reoriented to give a saturation moment that amounts to only $\frac{1}{4}$ of the moment per Yb. Since the Yb moment cannot be larger than $\approx 4.5\mu_B$/Yb, the saturation magnetization predicted in this configuration is much smaller than the measured value.

The third scenario takes domain 1 to have half the Yb moments perpendicular to the (110) bonds and half parallel to the (-110) bonds, so that all moments can be reoriented by an external field along 110 to give the correct saturation moment of $\approx 1/2$ of $4\mu_B$/Yb. Domain 2 consists of the opposite configuration where moments are perpendicular to the (110) bonds and parallel to the (-110) bonds, i.e., it is domain 1 rotated by 90°. An external field along (110) will leave domain 2 unaffected. Here, the moments parallel to the dimer bonds do not contribute to the magnetic diffraction intensity, and our simulations concur that the refined AF moment is too small by a factor of 2, both in zero and nonzero fields.

Our conclusion is that the two-domain scenario is overconstrained, due to the combination of the lattice of orthogonal bonds where the Ising moments can only be parallel or antiparallel to these bonds. The crystal structure (Fig. 1) motivates our adoption of a structure where $\mathbf{q_1} = (0.2,0.2,0)$ and $\mathbf{q_2} = (-0.2,0.2,0)$ define two orthogonal moment sublattices in the SSL plane, each containing half of the Yb moments, as we described above. The fourth $(1+\delta,1+\delta,1)$ satellite around (111) is much weaker than can be explained by either the Yb magnetic form factor or self-absorption corrections, and this reduced intensity will be captured by our magnetic structure model as well. We will show that this scenario fully reproduces the magnetic diffraction intensities, as well as the saturation magnetization and its anisotropy that was discussed above. From a wholly experimental perspective, the presence of two antiferromagnetic domains would likely also lead to significant hysteresis in the temperature dependencies of the low field magnetic susceptibility when the sample is cooled into the antiferromagnetic state in either zero field [zero field cooled (ZFC)] or in a field that is larger than $\simeq 3$ T [field cooled (FC)], the saturation field. Our measurements find no evidence for hysteresis in the ZFC or FC susceptibilities $\chi(T)$, or in the field dependence of the magnetization $M(B)$, other than near the quantized magnetization steps [18–20].

Previous magnetization measurements are consistent with the Yb moments being either parallel or perpendicular to the (110) and (-110) dimer bonds [17,33]. The direction of the magnetic moments in Yb_2Pt_2Pb is not constrained by symmetry considerations, but our model of the magnetic structure produces no AF peaks when the moments are oriented along the dimer bonds. We conclude that the Yb moments in Yb_2Pt_2Pb are oriented perpendicular to their own dimer bonds, so the $\mathbf{q_1} = (0.2,0.2,0)$ sublattice is formed by dimers oriented along (110) with perpendicular moments along (-110) and for the orthogonal $\mathbf{q_2} = (-0.2,0.2,0)$ sublattice the dimers are along (-110) with moments along (110).

The magnetic structure of Yb_2Pt_2Pb is obtained from the refinement of neutron diffraction data obtained on a 5 g powder using BT-7. The 10 K neutron powder pattern [Fig. 5(a)] is well refined using the reported U_2Pt_2Sn-type tetragonal structure [34]. The 0.5 K neutron powder diffraction pattern has additional peaks corresponding to AF order [Fig. 5(a)], also evident in the data obtained on the 6 g aligned crystal array using CNCS [Figs. 4 and 5(b)]. The $(1\pm\delta,1\pm\delta,0)$ satellites in the $(HH0)$ scan in Fig. 5(b) arise from Yb moments that are perpendicular to $(HH0)$, i.e., to the AF propagation direction $\mathbf{q_1}$. We performed no scans along directions parallel to $(-HH0)$, however, we have added for clarity the second set of AF satellites that arise from the moments perpendicular to $\mathbf{q_2}$. The 1.5 K $(HH0)$ neutron scan [Fig. 5(c)] shows that two satellite peaks flank each of the (110), (220), and (330) nuclear Bragg peaks. Their absence in x-ray scans carried out on the same crystal [Fig. 5(c)] indicates that there is no appreciable structural distortion at T_N.

The magnetic structure in Yb_2Pt_2Pb is quite complex, involving two different AF wave vectors and the formation of a $5\times5\times1$ supercell with 200 Yb moments. Conventional representation analysis shows that preserving the independence of the two AF sublattices within the U_2Pt_2Sn structure requires that no more than eight of the 16 symmetry operators of $P42/mmm$ may be retained in the magnetic space group. P1 and P-1 are the only space groups that contain any subset of these eight elements, but irreducible representations of these groups place no constraints on the coefficients of the basis

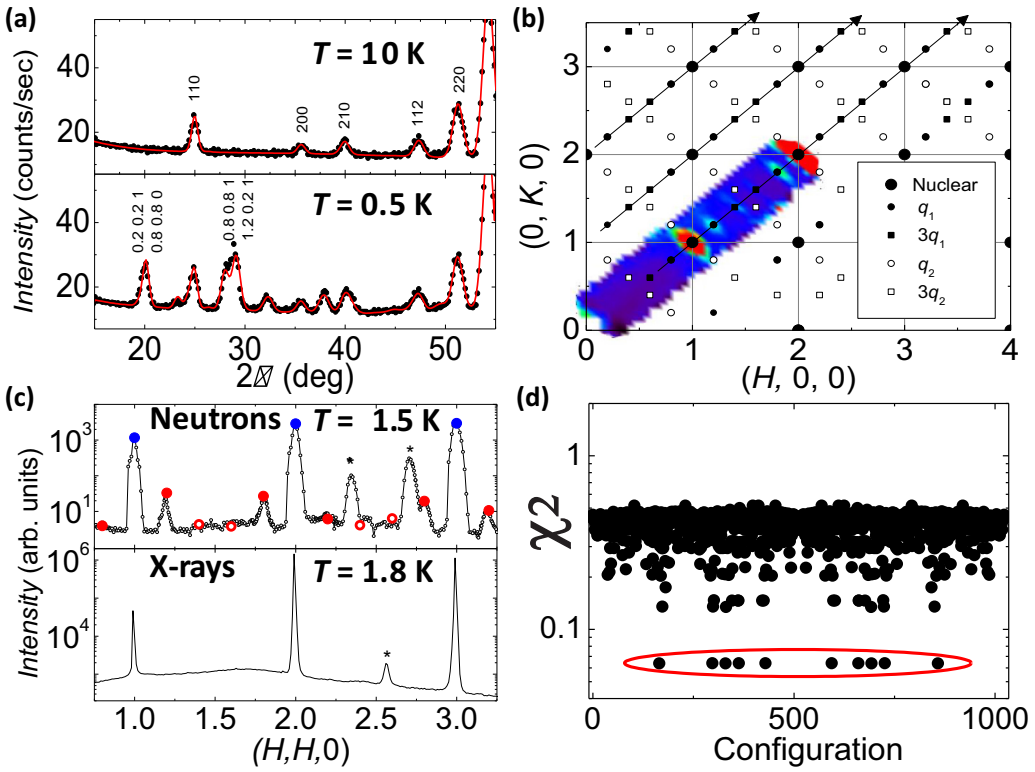

FIG. 5. (a) Neutron powder diffraction patterns at 10 K (top) and 0.5 K (bottom), with selected AF and nuclear Bragg peaks marked by Miller indices. Red lines are profile-matched Rietveld fits described in the text. (b) Schematic plot of $HK0$ plane for $T \leqslant T_N = 2.07$ K, indicating nuclear • and main AF satellites $\mathbf{q_1}$ (•) and $\mathbf{q_2}$ (○), as well as AF harmonics $3\mathbf{q_1}$ (■) and $3\mathbf{q_2}$ (□). A ($HK0$) scan taken from CNCS data (1.5 K, 0 T) is overplotted. (c) Neutron (BT-7, 1.5 K, top) and x-ray (X21, 1.8 K, bottom) $HH0$ scans of 0.06 g single crystal. Stars indicate extrinsic Al peaks. Filled blue points indicate nuclear intensities, while full(open) red circles indicate intensities of first order (first harmonic) AF satellites predicted by our magnetic model. (d) Residual χ^2, defined in text, for 1024 possible stripe configurations. Red circle encloses the 10 solutions with lowest $\chi^2 = 0.064$.

vectors that define the magnetic moments. As a consequence, we have taken another approach to formulating the magnetic structure of Yb_2Pt_2Pb, where the strong Ising character of the Yb moments plays a central role. The crystal structure consists of both Yb1 and Yb2 dimers in the SSL planes, potentially having different Yb moments $M1$ and $M2$. As shown in Figs. 1(c) and 1(d), the unit cell contains $z = 0$ and $z = 1/2$ planes with both types of dimers, but they are staggered along the c axis so that a Yb1 dimer with Yb moment $M1$ ($z = 0$) is always below a Yb2 dimer with Yb moment $M2$ ($z = 1/2$), thus forming corrugated ladders due to the length differences of the two types of dimer rungs.

We take these Yb dimers as the building blocks of the magnetic structure. Since the Yb moments of the crystal-field doublet ground state are large and classical, we consider here the four configurations of two distinguishable moments (Fig. 6), i.e., ↑↓, ↓↑, ↑↑, and ↓↓, and not the singlet-triplet states of two indistinguishable quantum spins as in $SrCu_2(BO_3)_2$. The AF state consists of two identical and interleaving magnetic sublattices in each SSL plane, oriented perpendicular to each other [Figs. 6(a) and 6(b)]. Inspired by the stripelike structures found in $SrCu_2(BO_3)_2$ at high fields [7,8,35], we construct the $5 \times 5 \times 1$ AF superlattice of Yb_2Pt_2Pb from stripes that contain a single configuration of Yb pairs, with the dimer bonds along (110) and moments parallel to (−110) for the sublattice with $\mathbf{q_1} = (0.2,0.2,0)$ and with dimer bonds along (−110) and moments parallel to (110) for the perpendicular sublattice with $\mathbf{q_2} = (-0.2,0.2,0)$ (Fig. 6). Each SSL plane consists of two perpendicular arrangements of dimer stripes, and both orthogonal sublattices are present in the $z = 0$ and $z = 1/2$ planes [Figs. 6(a) and 6(b)]. The principal AF wave vectors $(\pm 0.2,0.2,1)$ indicate there must be a net AF alignment of the neighboring $z = 0$ and $z = 1/2$ planes that comprise the chemical unit cell (Figs. 4 and 5). The weak $(\pm 0.2,0.2,0)$ reflections in Fig. 5(b) result from the incomplete compensation of the unit cell magnetic structure factor for $L = 0$ due to the corrugated ladder geometry. For instance, if there is a moment bearing ↑↑ dimer stripe in the $z = 0$ plane [Fig. 6(a)], there must be an antiparallel moment bearing ↓↓ dimer stripe in the neighboring $z = 1/2$ plane [Fig. 6(b)]. Similarly, stripes of ↑↓ dimers in the $z = 0$ plane must be stacked beneath stripes of ↓↑ dimers in the $z = 1/2$ plane. For both sublattices and in both $z = 0$ and $z = 1/2$ planes, stripes based on each of the four dimer configurations can be arranged in a total of 1024 different ways within the $5 \times 5 \times 1$ AF supercell of Yb_2Pt_2Pb.

Each of these 1024 stripe configurations was refined against the 0.5 K neutron powder data [Fig. 5(a)] using FULLPROF [36]. The Yb form factor was included in the refinements, in which only two parameters, the Yb moments on the Yb1 and Yb2 dimers $M1$ and $M2$, were varied. The computed diffraction patterns were subtracted from the 0.5 K diffraction

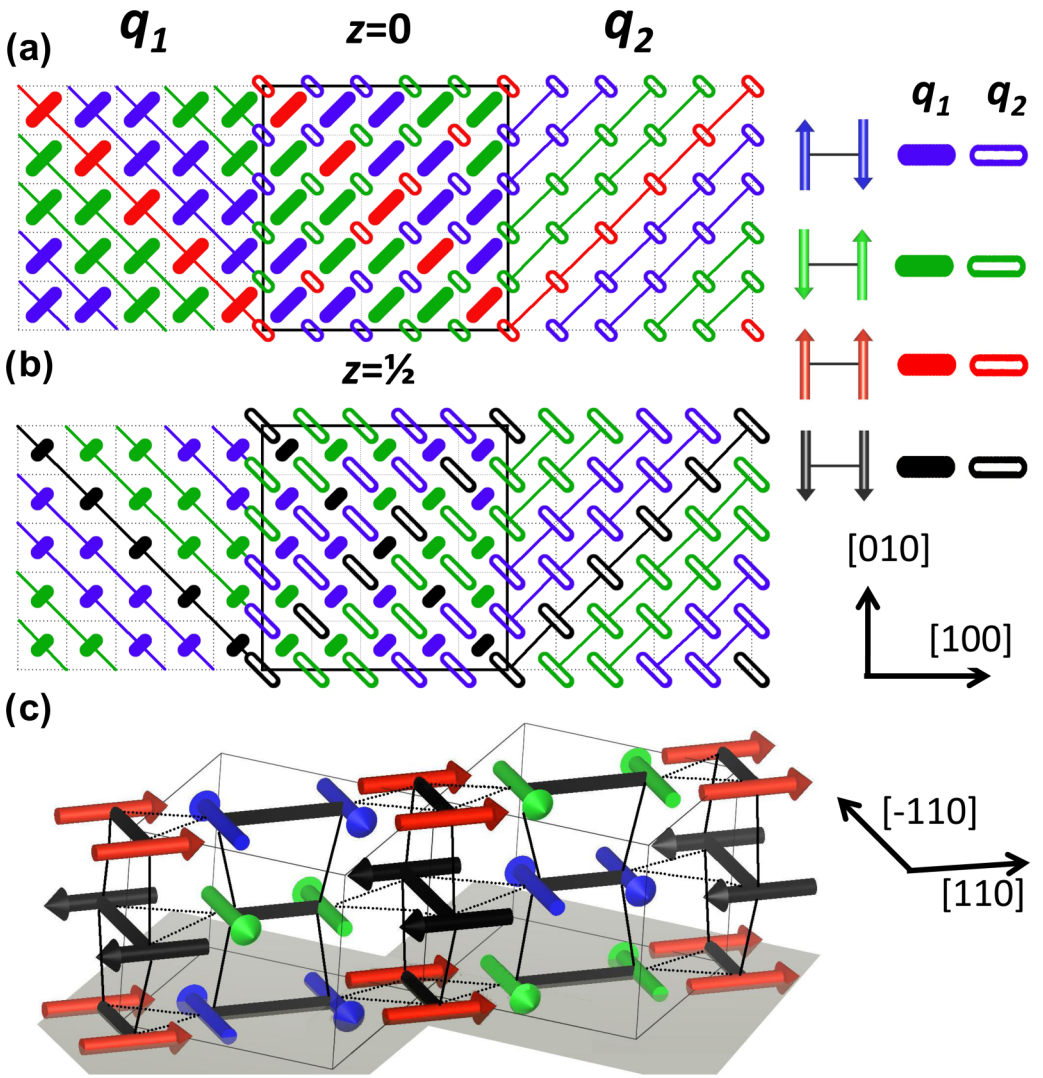

FIG. 6. Key: the four configurations of classical Yb dimers, on the $\mathbf{q_1}$ (filled symbols) and $\mathbf{q_2}$ (open symbols) sublattices. Symbols are elongated in the direction of the dimer bond; larger (smaller) symbol sizes indicate long (short) dimers. The $z = 0$ (a) and $z = 1/2$ (b) planes are formed by interleaving orthogonal $\mathbf{q_1}$ (left) and $\mathbf{q_2}$ (right) sublattices, to form the $5 \times 5 \times 1$ AF supercell (solid lines, center panels). Each sublattice consists of ordered sequences of stripes consisting of single dimer types (different colors). (c) A fragment of the complete magnetic structure, showing AF stacking of short and long dimers along the c axis.

pattern to generate a residual χ^2 for each stripe configuration. Figure 5(d) shows that there are ten configurations that have markedly smaller values of $\chi^2 = 0.064$, consisting of the five permutations of the stripe sequence $(\uparrow\downarrow,\uparrow\downarrow,\downarrow\uparrow,\downarrow\uparrow,\uparrow\uparrow)$ and its mirror reflection $(\downarrow\uparrow,\downarrow\uparrow,\uparrow\downarrow,\uparrow\downarrow,\downarrow\downarrow)$ [Figs. 6(a) and 6(b)]. The fit converged to have the same Yb moment on every site, $M1 = M2 = 3.8 \pm 0.2\mu_B$/Yb, which is in excellent agreement with the $3.95\mu_B$/Yb predicted above by the point charge model for Yb in the $|\pm 7/2\rangle$ Kramers doublet ground state, as well as the measured saturation moment M_{110} [17,33]. The simulated powder pattern with the lowest χ^2 agrees very well with the 0.5 K powder pattern [Fig. 5(a)]. We also computed specific nuclear and AF peak intensities from this magnetic solution, finding excellent agreement with the peak heights found in the 0.5 K $(HH0)$ single crystal scan [Fig. 5(c)]. The Supplemental Material [37] contains a file of the neutron diffraction intensity for Yb_2Pt_2Pb at $T = 0.5$ K, and its statistical error as a function of the scattering angle. It is provided so that a comparison of alternative models could be made by other authors.

The refined magnetic structure for Yb_2Pt_2Pb is remarkably intricate (Fig. 6). Both sublattices in each SSL layer are net-moment bearing, containing individual $\uparrow\uparrow$ or $\downarrow\downarrow$ stripes, spatially separated by two pairs of magnetically compensated $\downarrow\uparrow$ or $\uparrow\downarrow$ stripes for a total of five stripes per magnetic unit cell. The moment-bearing stripes in neighboring SSL layers are arranged AF along the c axis, and a fragment of the $5 \times 5 \times 1$ magnetic unit cell is depicted in Fig. 6(c) to emphasize the full three-dimensional magnetic structure of Yb_2Pt_2Pb. The Ising character of the Yb moments requires there to be two identical but orthogonal sublattices in each SSL layer, where half of the moments are parallel to (110) and the other half to (−110). Consequently, only the $\mathbf{q_1}$ sublattice, which has dimer bonds along (110) and moments perpendicular to (110), will be saturated by fields in the (−110) direction. The AF peaks associated with the $\mathbf{q_2}$ sublattice are unaffected by

field [Fig. 4(d)], as is the phase line $T_N(B) = 2.07$ K [33], demonstrating that the two sublattices can be considered independent.

While the structure that is sketched in Fig. 6 is quite complex, a number of its essential features can be rationalized by assuming that it is the consequence of dipolar interactions among Yb moments where strict Ising anisotropy limits the moments to be perpendicular to the dimer bonds. In general terms, the dipolar interaction favors the antiferromagnetic alignment of moments in directions perpendicular to the moment direction, and ferromagnetic alignment along the moment direction itself. Within a single dimer in the SSL plane, the antiparallel moment configurations ($\uparrow\downarrow$ and $\downarrow\uparrow$) are favored. In this way, the stripes consisting of parallel moment configurations ($\uparrow\uparrow$ and $\downarrow\downarrow$) can be considered to be domain walls that are required to sustain the 5×5 commensurability in the SSL plane. The origin of the dimer stripes of coaligned moments can also be understood as a consequence of dipolar interactions, since here the moments and the stripe direction are parallel, leading to a preferred ferromagnetic alignment of the dimers along the stripe direction, just as is observed in Figs. 6(a) and 6(b). Our magnetic structure is also consistent with the decoupling of the two sublattices that was evidenced by the magnitude of the saturation magnetization [Fig. 3(a)], and by the observation that only the antiferromagnetic satellites with wave vectors perpendicular to the field survive in high fields [Figs. 4(c) and 4(d)]. Specifically, our magnetic structure has neighboring AF dimers along the direction of the dimer bonds. The nearest neighbor moments 1 and 3, each on different dimers on the same sublattice 1, are consequently parallel. Located in between moments 1 and 3 on sublattice 1 is moment 2, which lies on the orthogonal sublattice 2. Regardless of the direction of moment 2, the geometry of the SSL plane ensures that the interaction between moments 1 and 2 has the same magnitude but the opposite direction of the interaction between moments 3 and 2. We conclude that there is no net dipolar interaction between moments on orthogonal sublattices, and that they can consequently be considered to be decoupled. This too is in good agreement with the experimental evidence presented above, that the two sublattices can be independently magnetized. Finally, we turn to the magnetic structure along the c axis, and since this direction is perpendicular to the moments, which are strictly limited to lie in the SSL planes, this implies an antiferromagnetic alignment of nearest neighbor dimers between SSL layers, as depicted in Fig. 6(c). Given that the shortest interdimer spacing is along the c axis, the dipolar interactions could be expected to be strongest in the direction perpendicular to the SSL planes. If so, Yb_2Pt_2Pb might best be thought of as a system of orthogonal and staggered spin ladders with rungs that are formed from the bonds of the SSL. While these qualitative arguments indicate that dipolar interactions are likely to be responsible for the main features of the observed magnetic structure in Yb_2Pt_2Pb, our estimates of the magnitudes of these dipolar interactions indicate that they cannot, by themselves, be responsible for long range magnetic order at the Neéel temperature of 2.07 K. A scenario where a stronger interaction, such as exchange, reinforces the dipolar exchange along the c axis, resulting in spin ladders that are weakly coupled by dipolar interactions, is one alternative that could resolve this dilemma.

Consistent with the Ising character of the Yb moments in Yb_2Pt_2Pb, the directions but not the magnitudes of the Yb dimer moments are modulated by a square wave with a periodicity of five chemical unit cells in the SSL plane. In addition to the fundamental modulation with $\delta = 0.2$, we have also observed 3δ harmonics in the $(HH1)$ scans obtained on the 6 g array of aligned crystals at 1.5 K (CNCS) and at 0.1 K (DCS) [Fig. 7(a)]. The ratio of the $(\delta,\delta,1)$ AF peak to the $(3\delta,3\delta,1)$ harmonic is 0.122 in our model, in good agreement with the experimental data at 0.1 K. While the model correctly estimates the intensities of the nuclear and main AF peaks at 1.5 K, the 3δ harmonics are much weaker than predicted, implying the presence of longitudinal fluctuations with a temperature dependence that follows that of the order parameter. The specific heat C/T, and the temperature derivatives of the electrical resistivity $\rho(T)$ and magnetic susceptibility $\chi(T)$ [Fig. 7(b)] all show peaks with the onset of AF order at $T_N = 2.07$ K, as well as an additional broad feature that is centered at $\simeq 0.8$ K. $\rho(T)$ was measured with the current along the c axis and with a magnetic field oriented along (110), and it is plotted with its temperature derivative $\partial\rho/\partial T$ in Fig. 7(c) for $B = 0$, 1 T, and 5 T. It is striking that the ordering anomaly remains fixed at $T_N = 2.07$ K, indicating that $\rho(T)$ is affected by the ordering of the Yb moments of the $\mathbf{q_1}$ sublattice, even when the $\mathbf{q_2}$ sublattice has been fully polarized by the 5 T field. While the general appearance of the broad maximum in $\partial\rho/\partial T$ changes slightly in field, it remains centered at 0.8 K in all fields.

The picture that emerges from the data in Fig. 7 is that individual Yb dimers form above T_N, consistent with the intradimer exchange $J \simeq 0.6$ meV that was deduced from fits to $\chi(T)$ [18]. As $T \to T_N$, these dimers assemble into a stripelike magnetic structure, accompanied by the gradual transfer of spectral weight from critical fluctuations into static order. The freezing out of these longitudinal fluctuations between 1.5 and 0.1 K and the much stronger temperature dependencies in C/T and the temperature derivatives of $\chi(T)$ and $\rho(T)$ above 0.8 K are together indications that these critical modes are gapped by $\Delta E/k_B \simeq 0.8$ K, where k_B is Boltzmann's constant. The magnetic structure proposed here is based on the neutron powder data obtained at 0.1 K, where the foundational assumption of fully Ising moments in our magnetic model is validated by the quality of the agreement with the measured data. We do not propose here a full description of the data at 1.5 K, where we must consider the possibility of a structure where the Yb moments as well as their direction have a slight amplitude modulation, possibly reflecting rounding of the edges of the magnetic stripes as a precursor of the collapse of antiferromagnetic order at T_N.

The magnetic structure of Yb_2Pt_2Pb is based on stripes consisting of different moment-bearing and magnetically compensated configurations of Yb moments with strong Ising-like single ion anisotropy. In some ways, it is reminiscent of the striped order found by nuclear magnetic resonance experiments in $SrCu_2(BO_3)_2$ [8,9], where increasing fields drive the SSL dimers based on Cu-based $S = 1/2$ quantum spins through a sequence of discrete patterns of singlet

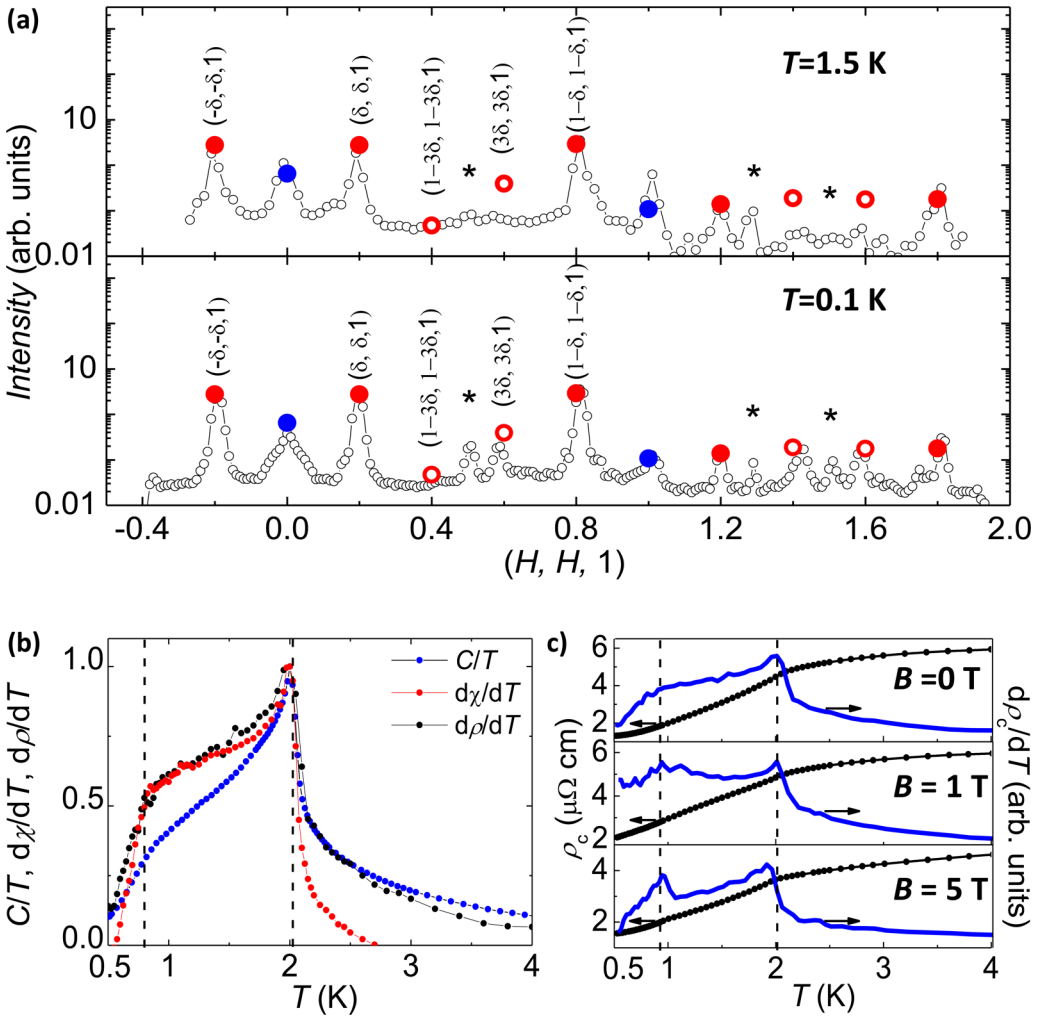

FIG. 7. (a) $(HH1)$ scans at 1.5 K (top, CNCS) and 0.1 K (bottom, DCS). Blue circles are nuclear intensities, filled (open) red points are fundamental (first harmonic) AF intensities predicted by our magnetic model, and ⋆ marks Al peaks. (b) Temperature dependencies of the specific heat C/T, and the temperature derivatives of ρ and χ, the latter measured in a dc field of 0.1 T. All data are normalized at $T_N = 2.07$ K to emphasize similar temperature dependencies. (c) $\rho(T)$ and $\partial\rho/\partial T$ at different fields $B\|(110)$. Vertical dashed lines in (b) and (c) are at $T_N = 2.07$ and 0.8 K.

and triplet states, reflecting the frustration of short-ranged exchange interactions inherent to the SSL [7,35]. While we do not mean to imply there is a formal correspondence between the magnetic structures in high field $SrCu_2(BO_3)_2$ and Yb_2Pt_2Pb in zero field, we find a much larger separation between the moment-bearing stripes in metallic Yb_2Pt_2Pb, suggesting that here the frustration may be embodied in the long-ranged dipole interactions on the SSL lattice, as well as the Ruderman-Kittel-Kasuya-Yosida interactions, mediated by the conduction electrons. The low fields required for the suppression of AF order, for the cascade of magnetization steps that suggest intermediate structures of magnetic and nonmagnetic dimers [19,20], and for the saturation of the individual sublattices in Yb_2Pt_2Pb may permit future investigations of the intermediate field states using neutron scattering, currently impossible in $SrCu_2(BO_3)_2$ where fields approaching 30 T are required to drive analogous modulated phases [10–12].

The strong Ising anisotropy that restricts the Yb moments to lie along the (110) and (−110) directions has far-reaching implications for the magnetic order found in Yb_2Pt_2Pb. Unlike $SrCu_2(BO_3)_2$ and also TmB_4 [14], where the moments are perpendicular to the SSL planes with a single AF wave vector, two perpendicular sublattices are required in Yb_2Pt_2Pb to accommodate the Ising moments [33], which can be independently polarized by fields in the SSL plane. Once one sublattice is fully polarized, the SSL motif of orthogonal dimers is destroyed in favor of a square lattice of the remaining Yb dimers with spacing that approaches 8 Å, while maintaining the same value $T_N = 2.07$ K that was found at $B = 0$ when both sublattices order. This is a very different AF state than has been envisaged for SSL systems with Heisenberg spins [3], and it is likely that SSL physics does not act alone in determining the underlying structure and excitations of Yb_2Pt_2Pb.

We acknowledge valuable discussions with T. Sakakibara. Work at Stony Brook University (W.M., L.S.W., M.S.K., T.O., J.W.S., D.M., M.C.A.) was supported by NSF-DMR-1310008. Work at BNL (M.G., I.Z., A.M. T.) and use of the NSLS were

supported by Office of Basic Energy Sciences (BES), Division of Materials Sciences and Engineering, U.S. Department of Energy (DOE), under Contract No. DE-SC00112704. This work utilized facilities supported in part by the National Science Foundation under Agreement No. DMR-0944772. Research conducted at SNS was sponsored by the Scientific User Facilities Division, Office of Basic Energy Sciences, U.S. Department of Energy.

[1] T. M. Rice, Science **298**, 760 (2002).
[2] L. Balents, Nature (London) **464**, 199 (2010).
[3] B. Sutherland and B. S. Shastry, Physica **1088**, 1069 (1981).
[4] S. Miyahara and K. Ueda, J. Phys.: Condens. Matter **15**, R327 (2003).
[5] B. D. Gaulin, S. H. Lee, S. Haravifard, J. P. Castellan, A. J. Berlinsky, H. A. Dabkowska, Y. Qiu, and J. R. D. Copley, Phys. Rev. Lett. **93**, 267202 (2004).
[6] K. Kakurai, K. Nukui, N. Aso, M. Nishi, H. Kadowaki, H. Kageyama, Y. Ueda, L.-P. Regnault, and O. Cépas, Prog. Theor. Phys. Suppl. **159**, 22 (2005).
[7] T. Momoi and K. Totsuka, Phys. Rev. B **62**, 15067 (2000).
[8] K. Kodama, M. Takigawa, M. Horvatic, C. Berthier, H. Kageyama,Y. Ueda, S. Miyahara, F. Becca, and F. Mila, Science **298**, 395 (2002).
[9] M. Takigawa, M. Horvatić, T. Waki, S. Krämer, C. Berthier, F. Lévy-Bertrand, I. Sheikin, H. Kageyama, Y. Ueda, and F. Mila, Phys. Rev. Lett. **110**, 067210 (2013).
[10] Suchitra E. Sebastian, N. Harrison, P. Sengupta, C. D. Batista, S. Francoual, E. Palm, T. Murphy, N. Marcano, H. A. Dabkowska, and B. D. Gaulin, Proc. Natl. Acad. Sci, USA **105**, 20157 (2008).
[11] M. Jaime, R. Daou, S. A. Crooker, F. Weickert, A. Uchida, A. E. Feiguin, C. D. Batista, H. A. Dabkowska, and B. D. Gaulin, Proc. Natl. Acad. Sci. USA **109**, 12404 (2012).
[12] Y. H. Matsuda, N. Abe, S. Takeyama, H. Kageyama, P. Corboz, A. Honecker, S. R. Manmana, G. R. Foltin, K. P. Schmidt, and F. Mila, Phys. Rev. Lett. **111**, 137204 (2013).
[13] S. Michimura, A. Shigekawa, F. Iga, M. Sera, T. Takabatake, K. Ohoyama, and Y. Okabe, Physica B **378-380**, 596 (2006).
[14] K. Siemensmeyer, E. Wulf, H.-J. Mikeska, K. Flachbart, S. Gábani, S. Mat'aš, P. Priputen, A. Efdokimova, and N. Shitsevalova, Phys. Rev. Lett. **101**, 177201 (2008).
[15] S. Yoshii, T. Yamamoto, M. Hagiwara, S. Michimura, A. Shigekawa, F. Iga, T. Takabatake, and K. Kindo, Phys. Rev. Lett. **101**, 087202 (2008).
[16] S. Mat'aš, K. Siemensmeyer, E. Wheeler, E. Wulf, R. Beyer, Th. Hermannsdörfer, O. Ignatchik, M. Uhlarz, K. Flachbart, S. Gabáni, J. Phys.: Conf. Ser. **200**, 032041 (2010).
[17] M. S. Kim, M. C. Bennett, and M. C. Aronson, Phys. Rev. B **77**, 144425 (2008).
[18] M. S. Kim and M. C. Aronson, Phys. Rev. Lett. **110**, 017201 (2013).
[19] Y. Shimura, T. Sakakibara, K. Iwakawa, K. Sugiyama, and Y. Ōnuki, J. Phys. Soc. Jpn. **81**, 103601 (2012).
[20] K. Iwakawa, Y. Hirose, K. Enoki, K. Sugiyama, T. Takeuchi, F. Honda, M. Hagiwara, K. Kindo, T. Nakano, Y. Nozue, R. Settai, and Y. Ōnuki, J. Phys. Soc. Jpn. **81**, SB058 (2012).
[21] J. W. Lynn, Y. Chen, S. Chang, Y. Zhao, S. Chi, W. Ratcliff II, B. G. Ueland, and R. W. Erwin, J. Res. NIST **117**, 61 (2012).
[22] J. R. D. Copley and J. C. Cook, Chem. Phys. **292**, 477 (2003).
[23] E. Bauer and M. Rotter, *Book Series on Complex Metallic Alloys*, edited by E. Belin-Ferr (World Scientific, Singapore, 2009), Vol. 2.
[24] M. Rotter, M. D. Le, A. T. Boothroyd, and J. A. Blanco, J. Phys.: Condens. Matter **24**, 213201 (2012).
[25] K. W. H. Stevens, Proc. Phys. Soc. London, Sect. A **65**, 209 (1952).
[26] M. T. Hutchings, Solid State Phys. **16**, 227 (1964).
[27] D. L. Roach, D. K. Ross, J. D. Gale, and J. W. Taylor, J. Appl. Crystallogr. **46**, 1755 (2013).
[28] M. C. Aronson, M. S. Kim, M. C. Bennett, Y. Janssen, D. A. Sokolov, and L. Wu, J. Low Temp. Phys. **161**, 98 (2010).
[29] A. A. Aczel, L. Li, V. O. Garlea, J.-Q. Yan, F. Weickert, M. Jaime, B. Maiorov, R. Movshovich, L. Civale, V. Keppens, and D. Mandrus, Phys. Rev. B **90**, 134403 (2014).
[30] A. Fennell, V. Y. Pomjakushin, A. Uldry, B. Delley, B. Prévost, A. Désilets-Benoit, A. D. Bianchi, R. I. Bewley, B. R. Hansen, T. Klimczuk, R. J. Cava, and M. Kenzelmann, Phys. Rev. B **89**, 224511 (2014).
[31] J. I. Igarashi and T. Tonegawa, Phys. Rev. B **40**, 756 (1989).
[32] F. Heidrich-Meisner, I. A. Sergienko, A. E. Feiguin, and E. R. Dagotto, Phys. Rev. B **75**, 064413 (2007).
[33] A. Ochiai, S. Matsuda, Y. Ikeda, Y. Shimizu, S. Toyoshima, H. Aoki, and K. Katoh, J. Phys. Soc. Jpn. **80**, 123705 (2011).
[34] R. Pöttgen, P. E. Arpe, C. Felser, D. Kußmann, R. Müllmann, B. D. Mosel, B. Künnen, and G. Kotzyba, J. Solid State Chem. **145**, 668 (1999).
[35] S. Miyahara and K. Ueda, Phys. Rev. B **61**, 3417 (2000).
[36] J. Rodriguez-Carvajal, Commission on Powder Diffraction (IUCr) Newsletter **26**, 12 (2001).
[37] See Supplemental Material at http://link.aps.org/supplemental/10.1103/PhysRevB.93.104419 for neutron intensities as function of scattering angle 2Θ, which other researchers may wish to compare to alternative magnetic models.